ISSN 0036-0244, Russian Journal of Physical Chemistry A, 2016, Vol. 90, No. 7, pp. 1326–1333. © Pleiades Publishing, Ltd., 2016.

CHEMICAL KINETICS AND CATALYSIS

Hydroxylation of Phenol over MeAPO Molecular Sieves Synthesized by Vapor Phase Transport[1]

Hui Shao, Jingjing Chen, Xia Chen, Yixin Leng, and Jing Zhong

Jiangsu Key Laboratory of Advanced Catalytic Materials and Technology, School of Petrochemical Engineering, Changzhou University, Changzhou, 213164, China

e-mail: shaohui200800@cczu.edu.cn

Received March 27, 2015

Abstract—In this study, MeAPO-25 (Me = Fe, Cu, Mn) molecular sieves were first synthesized by a vapor phase transport method using tetramethyl guanidine as the template and applied to hydroxylation of phenol. The zeolites were characterized by XRD, SEM, FT-IR, and DR UV–Vis. As a result, MeAPO-21 and MeAPO-15 were synthesized by changing the Me/Al ratio. UV–Visible diffuse reflectance study suggested incorporation of heteroatoms into the framework and FT-IR study also supported these data. Effects of heteroatoms, contents of Me in MeAPO-25, reaction temperature, phenol/H_2O_2 mole ratios, reaction time and concentration of catalyst on the conversion of phenol, as well as on the selectivity were studied. FeAPO-25 exhibited a high catalytic activity at the mole ratio of FeO and Al_2O_3 equal to 0.1 in the synthesis gel, giving the phenol conversion of 88.75% and diphenols selectivity of 66.23% at 60°C within 3 h [n(phenol)/n(H_2O_2) = 0.75, m(FeAPO-25)/m(phenol) = 7.5%]. Experimental results indicated that the FeAPO-25 molecular sieve was a fairly promising candidate for the application in hydroxylation of phenol.

Keywords: heteroatom, MeAPO-25, vapor phase transport, phenol, hydroxylation

DOI: 10.1134/S0036024416070116

1. INTRODUCTION

In the family of aluminophosphate molecular sieves ($AlPO_4$-n), metal-containing aluminophosphate molecular sieves (MeAPOs) have received considerable interest due to their modified acid sites achieved by changing the metal amounts, large specific surface areas and great thermostability [1–3]. Up to now, $AlPO_4$-n molecular sieves have usually been synthesized in the hydrothermal or solvothermal systems by using organic amines as templates. Organic amines are toxic, inducing high production cost and environmental problems arising from the thermal decomposition of organic species [4]. Therefore, a lot of efforts have been made to find an environmentally friendly approach for the synthesis of crystalline aluminophosphates. Currently, an ionothermal synthesis method was reported for preparing molecular sieves using ionic liquids as both solvents and SDA, such as 1-butyl-3-methylimidazolium bromide ([bmim]Br) [5], a mixture of choline chloride (ChCl) and pentaerythritol [6], 1-ethyl-3-methylimidazolium bromide ([emim]Br) [7] etc. However, ionic liquids still suffered from a complex synthesis process and expensive cost. Low-toxic templates are urgently sought. Zhou et al. [8] used glucose mixed with triethylamine as the template to synthesize a hierarchical MeAPO-5 molecular sieve with mesopores and micropores. Wang et al. [9] used tetramethylguanidine (TMG) through conventional hydrothermal (CHT) method, successfully synthesized a typical $AlPO_4$-5. Nevertheless, friendly green templates have seldom been reported.

Typically, using the CHT method is required for separation between solvents and solid products, and partially organic SDAs are inevitably preserved in the liquid phase, resulting in the wastewater pollutants and downstream purification system installation [10]. To further optimize the synthesis technology to fit the principles of green chemistry, the synthesis of porous materials by vapor-phase transport (VPT) was first invented by Xu et al. [11]. Compared with CHT, VPT has many advantages over CHT, including reducing wastewater disposal, enhancing the efficiency of synthesis reactors and minimizing template dosages [12], resulting in lower production costs. In our previous work [13], Me-substituted aluminophosphate molecular sieves MeAPO-11 (Me = Cu, Fe, Zn, Mn) were synthesized by the VPT method using diisopropylamine as the template.

Hydroxylation of phenol with clean oxidants like H_2O_2 is a research topic of high industrial importance [14]. The products of hydroxylation of phenol can be

[1] The article is published in the original.

used as antioxidants, polymerization inhibitors [15], and photosensitive materials. Catalytic hydroxylation of diphenols has attracted large research attention [16]. Heteropoly acid salts, metallic oxides and molecular sieves containing heteroatoms had been used as the catalysts for this reaction [17–19]. At present, the uses of heteropoly acid salts depended on acetonitrile as the solvent, which has high toxicity and difficult recycling of catalysts. Although metal oxides have a low cost, convenient preparation and high stability, they were limited by a low selectivity. Hence, MeAPO-25 molecular sieves could be a potential competitor for the hydroxylation of Phenol.

The objective of this work was to develop a new method to synthesize MeAPO-25 (Me = Fe, Cu, Mn) by using the VPT method. Tetramethyl guanidine (TMG) was used as a friendly green template. The characteristics of MeAPO-25 molecular sieves, such as crystal structure and morphology, were studied. The catalytic performance of these MeAPO-25 molecular sieves was evaluated in the reaction of phenols hydroxylation. Additionally, the phase transition between MeAPO-21 and MeAPO-15 molecular sieves was observed by changing the metal content.

2. EXPERIMENTAL SECTION

2.1. Synthesis of MeAPO-25

MeAPO-25 molecular sieves were synthesized by using the VPT method. Mixtures with compositions of $1.3P_2O_5 : 1.0Al_2O_3 : x\text{MeO} : 1.0\text{TMG} : 100H_2O$ were used as precursors, where x was selected as 0.05 (a), 0.10 (b), 0.15 (c), 0.20 (d), or 0.25 (e). Pseudoboehmite was added to the distilled water, and stirred until a uniform gel was obtained. Phosphoric acid and TMG were added successively to the gel, which was stirred to a uniform reaction mixture. Then, cupric acetate, iron(II) sulfate septhydrate or manganese acetate tetrahydrate was added to the gel as the source of different metals, respectively. The resulted hydrogel was then dried at 80°C. The dry-gel powder was placed in a sample holder located in the middle part of an autoclave. A mixture of TMG and water (1 : 20 (vol/vol)) was placed at the bottom of the autoclave. The autoclave was then kept in the oven at 180°C for 24 h. The as-synthesized products were filtered, washed several times, dried and then calcined at 550°C.

2.2. Characterization

X-ray diffraction (XRD) experiments were performed on a Rigaku D/max2500 instrument with CuK_α radiation (40 kV, 100 mA). Scanning electron microscopy (SEM) images were collected on a S-3000N microscope at 30 kV. The FT-IR spectra of the samples were recorded as KBr disks on a PROTÉGÉ 460 spectrometer in the range of ~(4000–400) cm^{-1}. The diffuse reflectance UV–Vis spectra were obtained in the wavelength range of ~(200–800) nm on a VARIAN CARY-500 equipment. $BaSO_4$ was used as a reference.

2.3. Catalytic Test

Hydroxylation of phenol was conducted in a 100 mL round-bottomed flask. The reaction conditions were as follows: the reaction temperature was 60°C; the molar ratio of phenol to H_2O_2 was 0.75 : 1 (with 2.0 g phenol in 12.0 mL distilled water for the reaction); the mass of the catalyst was 0.1 g; and the reaction time was 3 h. The reaction was monitored by sampling periodically and analyzed using an EX-1600 series high performance liquid chromatography equipped with a C18 column (5 μm, 4.6 × 150 mm) and UV-detector (277 nm, 25°C).

3. RESULTS AND DISCUSSION

3.1. Synthesis of MeAPO with Different Metal Contents

Figure 1 shows the XRD patterns of as-synthesized samples of MeAPO (Fig. 1a) and the calcined forms of MeAPO (Fig. 1b). It clearly exhibits that the MeAPO-21 molecular sieves synthesized with different $n(\text{MeO})/n(Al_2O_3)$ ratios (Me = Fe, Mn) in the range of ~(0.05–0.25) have a typical AWO structure. The characteristic diffraction peak of the molecular sieves is the strongest with a MeO/Al_2O_3 ratio of 0.1. Then, the characteristic diffraction peak decreases with the increase of the metal content. This result indicates that the crystallinity decreases. The introduction of metal heteroatoms changes the chemical microenvironment near the crystal surfaces and affects the growth of the crystal faces. In addition, with the increase of the metals content, the non-framework species content increases. This changes the growth rate of the crystal faces, resulting in the reduced crystallinity of the molecular sieves [20]. The CuAPO-15 zeolite is synthesized with a small metal content. When the CuO/Al_2O_3 ratio reaches 0.25, the characteristic diffraction peaks of CuAPO-15 disappear.

In the XRD patterns of calcined MeAPO-21(Me = Fe, Mn) samples, the peak position and intensity are similar with the XRD patterns of $AlPO_4$-25 molecular sieves [21]. This suggests that the calcination transforms the MeAPO-21 molecular sieves into MeAPO-25 molecular sieves with a ATV structure. A structural unit of $AlPO_4$-21 molecular sieves has an AlO_4 tetrahedron, three PO_4 tetrahedra, and two AlO_5 trigonal bipyramids. Every two penta-coordinated aluminum ions result in an Al–O–Al connection, increasing the energy of the system. Based on the principle that the skeleton structure should be formed in accordance with the minimum energy of the system [22], the penta-coordinated aluminum in the framework of $AlPO_4$-21 is transformed into a tetra-coordinated form at high temperatures. Xiao et al. [23] pointed that

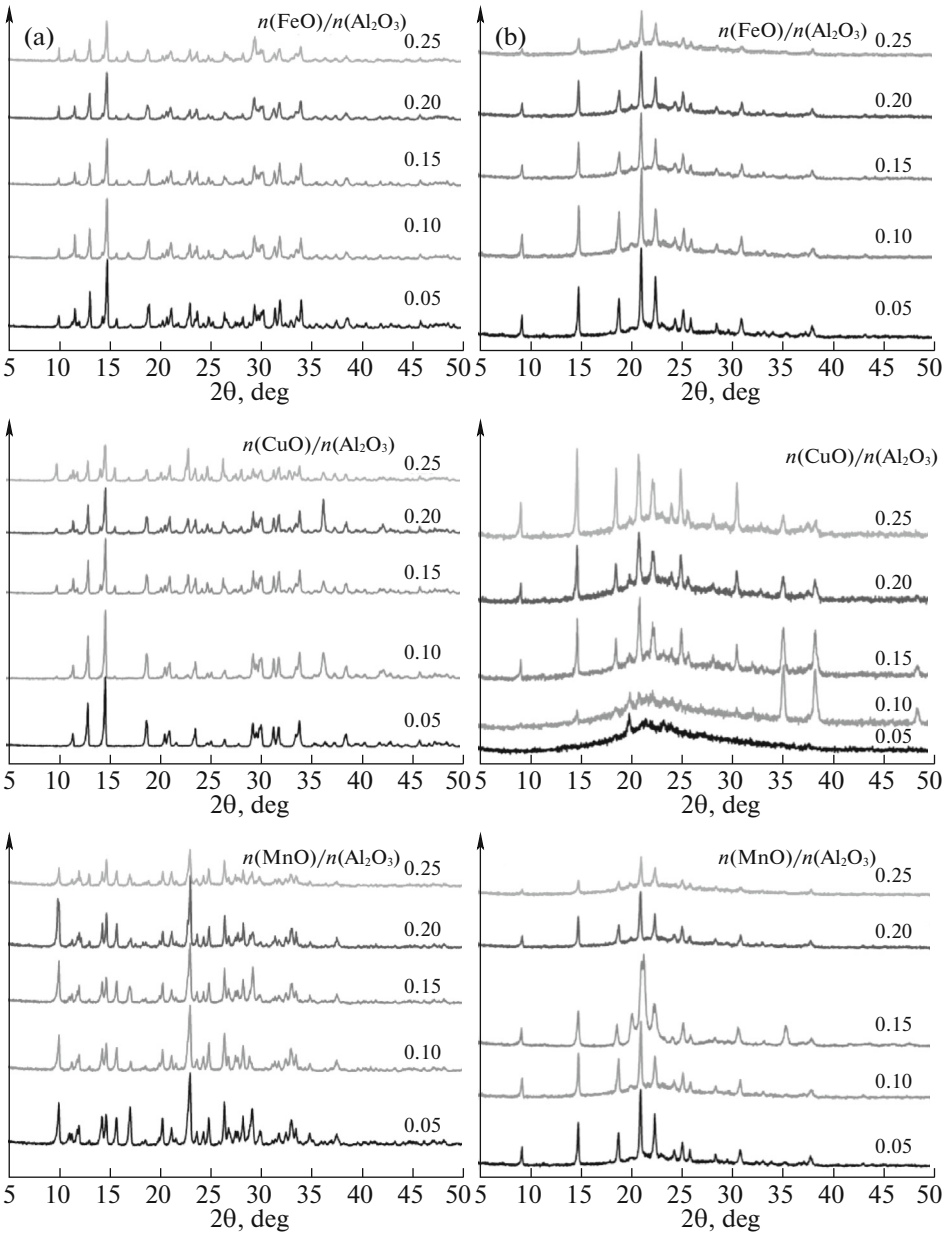

Fig. 1. XRD patterns of as-synthesized MeAPO (a) and calcined MeAPO (b) synthesized with different $n(MeO)/n(Al_2O_3)$.

the whole skeleton is transformed into $AlPO_4$-25 molecular sieves without changing the main channel of the eight-membered ring.

In the case of CuAPO-15, the XRD patterns of the CuAPO-15 molecular sieves after calcination do not show the characteristic diffraction peaks, indicating the presence of the amorphous state. It is consistent with the conclusion reported in the literature that the framework of $AlPO_4$-15 molecular sieve can be collapsed after calcination [24]. The CuAPO-21 molecular sieves are also transformed into CuAPO-25 molecular sieves. MeAPO-25 zeolites with a high crystallinity were employed as catalysts in the following study. The FeAPO-25 with the 0.10 FeO/Al_2O_3 ratio, the CuAPO-25 with the 0.25 CuO/Al_2O_3 ratio and the MnAPO-25 with the 0.10 MnO/Al_2O_3 ratio were characterized and applied to hydroxylation of phenol.

3.2. Characterization of MeAPO

SEM images of the as-synthesized and calcined FeAPO, CuAPO, and MnAPO molecular sieves are shown in Fig. 2. It shows that FeAPO-21 molecular sieves are about 15 × 15 μm in size (Fig. 2a). After calcination, the schistose crystals stack consists of irregular bulk particles. The CuAPO-21 molecular sieves (Fig. 2c)

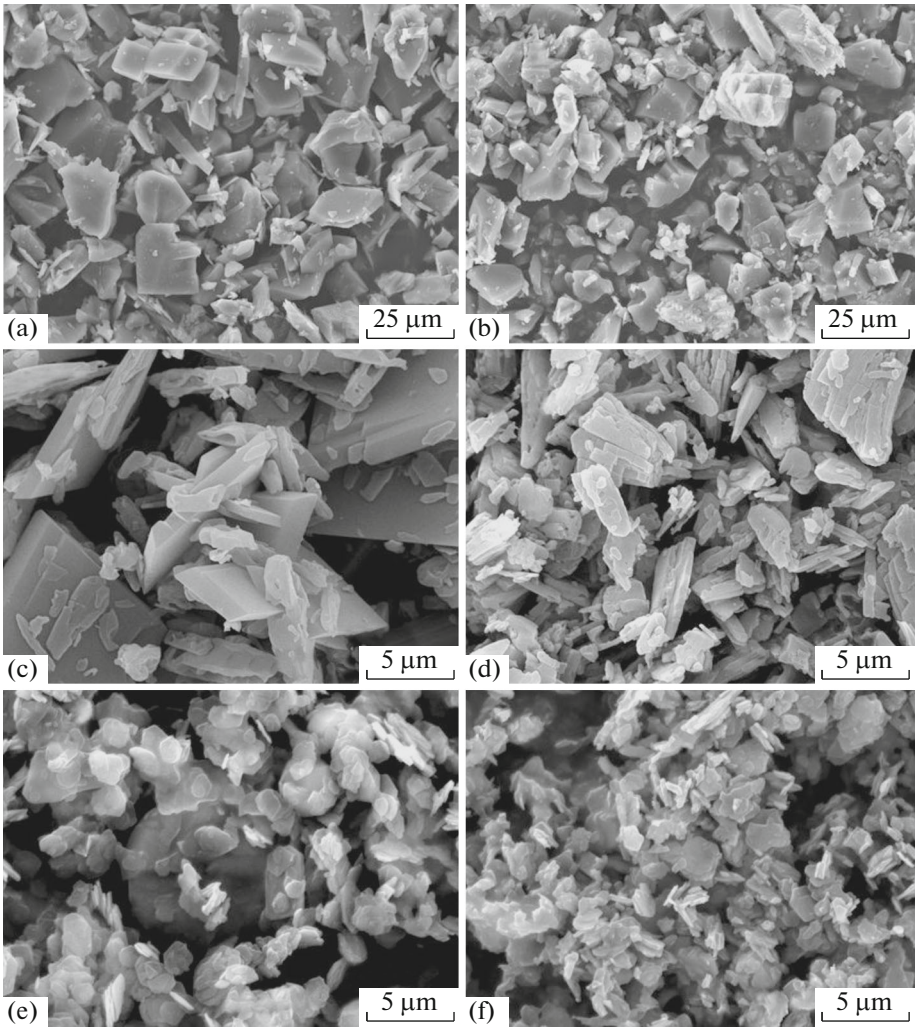

Fig. 2. SEM of the as-synthesized and calcined (a, b) FeAPO, (c, d) CuAPO, and (e, f) MnAPO.

are fine and smooth flake crystals with the size of ~(5–10) μm. The crystal size of CuAPO-25 is slightly larger than that of CuAPO-21. MnAPO-21 molecular sieves are spherical crystals with a diameter of about 2 μm piled by thin and small flake crystals (Fig. 2e). It is clear that the spherical crystals are destroyed after calcination. This also indicates that the form of the molecular sieve has changed in the calcination process.

UV–Vis spectra were recorded for the as-synthesized and calcined FeAPO, CuAPO, and MnAPO in order to identify the existence of metal ions in the framework or extra-framework of molecular sieves (Fig. 3). There was a very intense absorption band at about 260 nm in the spectra of as-synthesized FeAPO-21 as well as that of calcined FeAPO-25. This band was associated with the charge-transfer from ligand to metal [25]. This confirmed that Fe ions had been incorporated into the framework. Two bands at around 370–430 nm were observed for FeAPO-21 samples. These bands were usually attributed to the oxides of Fe presented in the extra-framework state. The absorption peak disappeared in the calcined FeAPO-25 molecular sieves, indicating the introduction of the heteroatoms into the frameworks. A characteristic band at ~(200–230) nm appeared in the spectra of both CuAPO-21 and CuAPO-25 due to the p–d electronic transition from the 2p electron of oxygen atoms to empty d-orbital of the heteroatom [26]. In the range of ~(300–480) nm there were no characteristic peaks, indicating that there were no heteroatom oxides in the extra-framework state of the as-synthesized and calcined samples. No absorption peak was observed for MnAPO-21 molecular sieves in the range of ~(190–230) nm, indicating that Mn atoms didn't exist in the frameworks.

FT-IR spectra of the as-synthesized MeAPO-21 molecular sieves (shown in Fig. 4) showed a new absorption band at 950 cm^{-1} [27] compared with the spectrum of $AlPO_4$-21. It illustrated heteroatom iso-

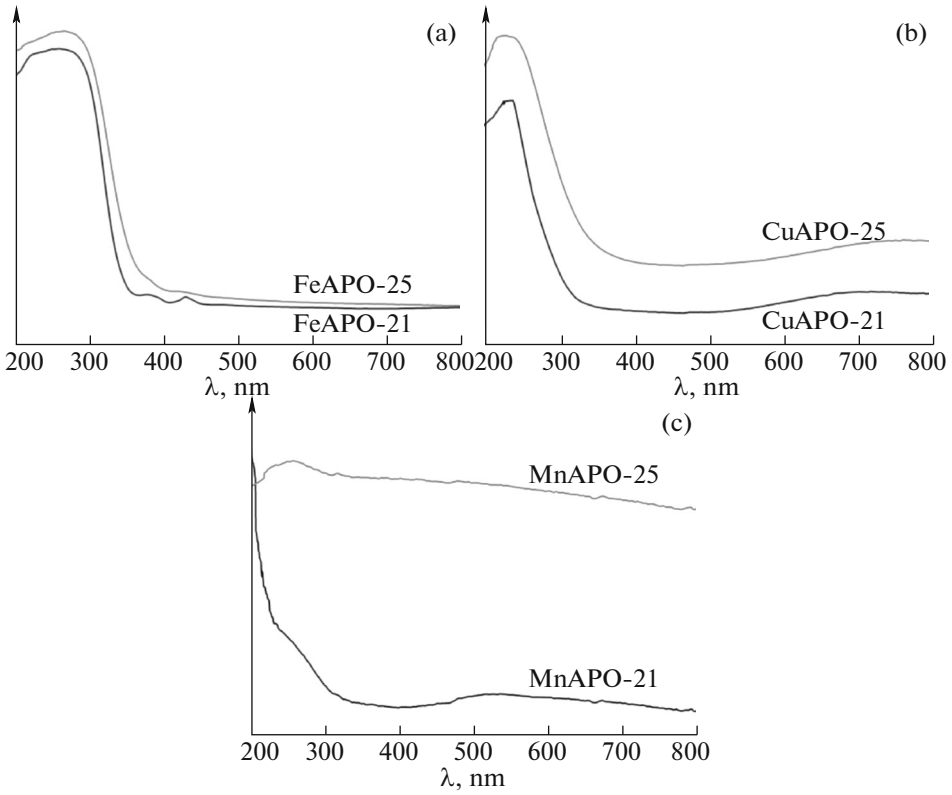

Fig. 3. DR UV–Vis spectra of the as-synthesized and calcined: (a) FeAPO, (b) CuAPO, and (c) MnAPO.

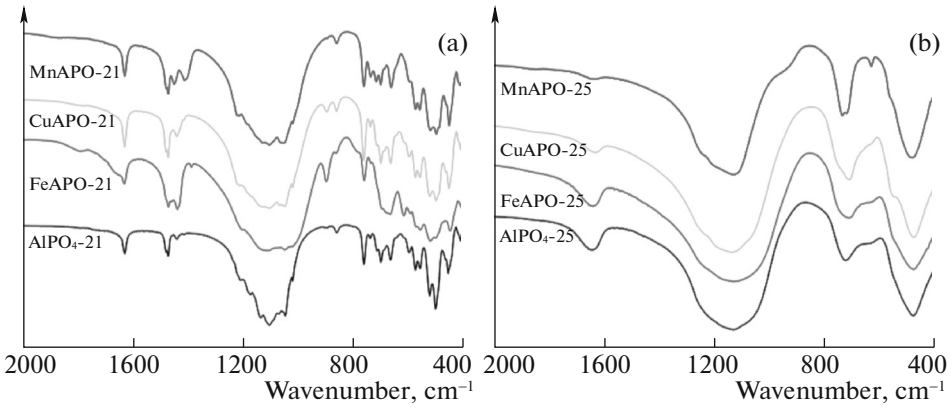

Fig. 4. FT-IR spectra of the as-synthesized MeAPO-21(a) and calcined MeAPO-25 (b).

morphous substitution of P or Al in the framework. On the other hand, this absorption band had a red shift compared to that of $AlPO_4$-21. This was attributed to the heavier atomic masses of Fe and Cu, compared with that of Al. With isomorphous substitution of Al with Fe or Cu, the M–O bond length became longer, leading to a red shift. But the spectrum of MnAPO-21 did not show the characteristic absorption at 950 cm^{-1}, clearly indicating that Mn atoms were in the extra-framework state. This was consistent with the conclusion of the UV–Vis spectroscopy. The FT-IR spectrum of the calcined MeAPO-25 molecular sieves led to a similar conclusion.

3.3. Catalytic Test

FeAPO-25, CuAPO-25, and MnAPO-25 molecular sieves were used as catalysts for hydroxylation of phenol. Their catalytic performances were illustrated in Fig. 5. FeAPO-25 showed a high activity in this reaction. At 60°C, the conversion of phenol reached 90% after 3 h, with the 66.23% diphenols selectivity.

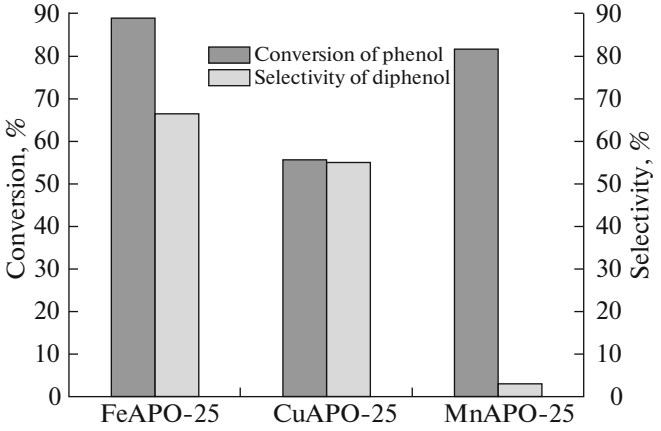

Fig. 5. The catalytic performance of MeAPO-25 in phenol hydroxylation (conditions: phenol 2.0 g, phenol/H_2O_2 molar ratio 3 : 4, water 12 mL, MeAPO-25 0.15 g, temperature 60°C, time 3 h).

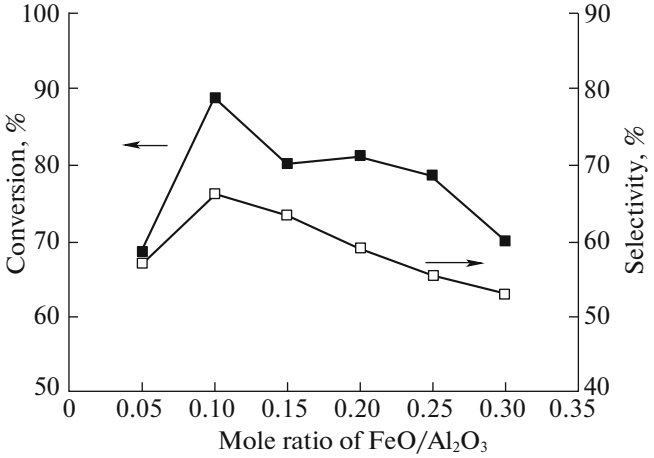

Fig. 6. Catalytic properties of FeAPO-25 with different contents of Fe for phenol hydroxylation (conditions: phenol 2.0 g, phenol/H_2O_2 molar ratio 3 : 4, water 12 mL, FeAPO-25 0.15 g, temperature 60°C, time 3 h).

MnAPO-25 favored a high conversion of phenol but with a low selectivity. As mentioned in the UV–Vis spectroscopy test, Mn species hardly enter into the framework of the molecular sieves. After calcination, Mn atoms in the pore were transformed into MnO_2. It is generally accepted that MnO_2 is the catalyst for the decomposition of H_2O_2 to O_2. Therefore, MeAPO-25 was excessively active for the phenol hydroxylation, diphenols were further oxidized and phenol was directly oxidized into tar. In addition, it has been reported that manganese oxides were excellent adsorbents for phenol [28]. The UV–Vis spectroscopy test also revealed that Fe^{3+} and Cu^{2+} ions entered the framework to form active centers of phenol hydroxylation. This might be affiliated with the acidity increase of catalysts after the modification with the metal. However, the acid sites of FeAPO-25 and CuAPO-25 should be further explored by FR-IR spectra of pyridine adsorption and NH_3-TPD for investigating the difference between FeAPO-25 and CuAPO-25. Reading these responses, further studies with different metal contents were carried out with FeAPO-25 molecular sieves.

The results of hydroxylation of phenol with different FeAPO-25 molecular sieves were presented in Fig. 6. It revealed that the phenol conversion and diphenol selectivity reached the maximum when the molar ratio of FeO and Al_2O_3 was 0.10. In the acid-catalyzed hydroxylation of phenol, the diphenols yield increased with the increase of the Fe content. Generally, aluminophosphate molecular sieves without any heteroatoms had few acid sites, which was useless for the phenol hydroxylation. Indeed, the more Fe atoms led to more acid activity, according to the Fe^{3+} atoms acted as active centers in the MeAPO-25 catalyst. However, Choi [29] had synthesized Fe-MCM-41 with varying amounts of Fe and it showed that small amounts of Fe in the synthesis gel would lead to a better formation of tetrahedral Fe species in the framework. This was in agreement with the result of XRD analysis. The catalytic activity decreased with the decrease of the zeolite crystallinity. Accordingly, the appropriate metal content was needed for the reaction of phenol hydroxylation.

Table 1. Effect of reaction variables on the phenol hydroxylation

Reaction variable	X_{Phenol}, %	S_{CAT}, %	S_{HQ}, %	S_{CAT+HQ}, %
Phenol/H_2O_2 ratio[a]				
0.5	88.27	23.22	31.57	54.79
0.75	88.75	28.09	38.14	66.23
1.0	72.03	28.32	39.87	68.19
1.25	59.77	29.26	40.21	69.47
Temperature (°C)[b]				
50	56.67	32.75	40.00	72.75
60	88.75	28.09	38.14	66.23
70	86.03	24.61	35.98	60.59
80	55.44	23.06	34.23	57.29
Time (h)[c]				
2	89.41	17.50	22.42	39.92
3	88.75	28.09	38.14	66.23
4	89.69	29.45	35.78	65.23
5	90.55	25.76	30.23	55.99

[a] Phenol 2.0 g, water 12 mL, FeAPO-25 0.15 g, temperature 60°C, time 3 h.

[b] Phenol 2.0 g, phenol/H_2O_2 molar ratio 3 : 4, water 12 mL, FeAPO-25 (b) 0.15 g, time 3 h.

[c] Phenol 2.0 g, phenol/H_2O_2 molar ratio 3 : 4, water 12 mL, FeAPO-25 (b) 0.15 g, temperature 60°C.

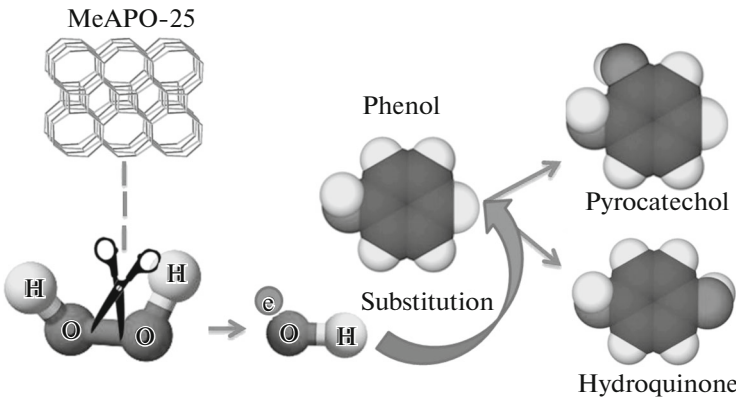

Fig. 7. Schematic diagram of phenol hydroxylation over the MeAPO-25 catalyst.

The influence of other reaction conditions such as the phenol/H_2O_2 ratio, reaction temperature and reaction time were studied by using FeAPO-25, and the results were shown in Table 1. In general, the conversion of phenol decreased with the increase of the phenol/H_2O_2 ratio, but the diphenols selectivity increased. Figure 7 illustrated the reaction mechanism of phenol hydroxylation over the FeAPO-25 catalyst. During the reaction, H_2O_2 was first decomposed to OH by the FeAPO-25 molecular sieve, then the •OH species reacted with phenol to produce catechol and hydroquinone. The increase of the H_2O_2 dosage led to the increase of the •OH concentration. Therefore, the conversion of phenol increased with increasing the amount of H_2O_2. However there was a competitive reaction for •OH: decomposition to H_2O and O_2. Further oxidation of diphenols by oxygen leads to the decrease of the diphenols selectivity.

The influence of the reaction temperature was studied in a range of ~(50–80)°C at an interval of 10°C. At 50°C, the conversion of phenol was very low compared with the conversion at 60°C. This might be due to the poor solubility of phenol. But Preethij [16] attributed this to the suppression of H_2O_2 chemisorption. With the further increase of temperature, both the conversion of phenol and diphenols selectivity decreased. It might be due to the activation energy of the reaction of •OH and phenol which was lower than the decomposition of •OH. Elevated temperatures favored the reaction with a high activation energy.

The effect of the reaction time was studied in a range of ~(0–5) h. The conversion of phenol kept unchanged and the diphenols achieved a maximum selectivity at 3 h. With further increasing of the reaction time, diphenols were further oxidized to produce the tar, due to a rapid decomposition of H_2O_2. Therefore, the optimal conditions of the reaction were: a phenol/H_2O_2 molar ratio of 0.75, temperature of 60°C and reaction time of 3 h, respectively.

FeAPO-25 molecular sieves, ranging from 2.5 to 10% (mass ratio, FeAPO-25/Phenol), were added into the solution of phenol. The catalytic results were listed in Table 2. With the increase of FeAPO-25 loading from 2.5 to 7.5%, the conversion of phenol increased from 57.12 to 88.75%. However, with a further increase in the amount of FeAPO-25, the conversion of phenol decreased. This is due to suitable acidity that can promote the formation of OH and the conversion of phenol. But if the acidity was too strong, the decomposition of •OH accelerated, decreasing the utilization of H_2O_2. Furthermore, after repeated use for three times, still a 64.93% phenol conversion and 40.51% diphenols selectivity were observed.

Table 2. Effect of catalyst dosage on the phenol hydroxylation over the FeAPO-25 catalyst[a]

w(FeAPO-25 (b))	X_{Phenol}, %	S_{CAT}, %	S_{HQ}, %	$S_{CAT + HQ}$, %
2.5	57.12	35.94	44.04	79.98
5	76.69	31.51	40.32	71.83
7.5	88.75	28.09	38.14	66.23
10	51.08	20.63	31.02	51.65

[a] Phenol 2.0 g, phenol/H_2O_2 molar ratio 3 : 4, water 12 mL, temperature 60°C, time 3 h.

CONCLUSIONS

In conclusion, MeAPO-25 molecular sieves (Me = Fe, Cu, Mn) were successfully synthesized by the VPT method using TMG as the template. MeAPO-25 molecular sieve could act as a catalyst to efficiently convert phenol to diphenols. The phenol conversion and diphenols selectivity were greatly affected by heteroatom species, metal content, the ratio of phenol/H_2O_2, reaction time, reaction temperature and the amount of the catalyst. The results indicated that Fe^{3+} and Cu^{2+} ions could be successfully incorporated into the framework of $AlPO_4$-25. But Mn^{2+} ions

hardly entered into the framework. An appropriate phenol conversion of 88.75% and diphenols selectivity of 66.23% had been achieved over the FeAPO-25 catalyst. FeAPO-25 molecular sieve could be used as an effective catalyst for the hydroxylation of phenol.

ACKNOWLEDGMENTS

This work is supported by National Natural Science Foundation (no. 21276029), the Perspective Research Foundation of Production Study and Research Alliance of Jiangsu Province of China (no. BY2014037-15). A Project funded by the Priority Academic Program Development of Jiangsu Higher Education Institutions (PAPD) and the project of overseas research plan for outstanding research group, young teachers and principals in Jiangsu Province.

REFERENCES

1. P.-S. E. Dai, R. H. Petty, C. W. Ingram, and R. Szostak, Appl. Catal. A: Gen. **143**, 101 (1996).
2. Q. Xingyi, Z. Lili, X. Wenhua, J. Tianhao, and L. Rongguang, Appl. Catal. A: Gen. **276**, 89 (2004).
3. M. Selvaraj, K. Seshadri, A. Pandurangan, and T. Lee, Microporous Mesoporous Mater. **79**, 261 (2005).
4. X. Huang, R. Zhang, and Z. Wang, Chin. J. Catal. **33**, 1290 (2012).
5. Z. Zhao, W. Zhang, R. Xu, X. Han, Z. Tian, and X. Bao, Dalton. Trans. **41**, 990 (2012).
6. X. Zhao, H. Wang, C. Kang, Z. Sun, G. Li, and X. Wang, Microporous Mesoporous Mater. **151**, 501 (2012).
7. R. Xu, W. Zhang, J. Xu, Z. Tian, F. Deng, X. Han, and X. Bao, J. Phys. Chem. C **117**, 5848 (2013).
8. L. Zhou, T. Lu, J. Xu, M. Chen, C. Zhang, C. Chen, X. Yang, and J. Xu, Microporous Mesoporous Mater. **161**, 76 (2012).
9. J. Wang, J. Song, C. Yin, Y. Ji, Y. Zou, and F. S. Xiao, Microporous Mesoporous Mater. **117**, 561 (2009).
10. J. Li, Z. Li, D. Han, and J. Wu, Powder Technol. **262**, 177 (2014).
11. W.-Y Xu, J.-X Dong, J.-P Li, J.-Q Li, and Feng Wu, J. Chem. Soc., Chem. Commun. **262**, 177 (1990).
12. C.-M. Song, Y. Feng, and L.-L. Ma, Microporous Mesoporous Mater. **147**, 205 (2012).
13. H. Shao, X. Chen, B. B. Wang, J. Zhong, and Y. Chao, Shiyou Xuebao, Shiyou Jiagong **28**, 933 (2012).
14. J.-N. Park, J. Wang, K. Y. Choi, W.-Y. Dong, S.-I. Hong, and C. W. Lee, J. Mol. Catal. A: Chem. **247**, 73 (2006).
15. L. Jian, C. Chen, F. Lan, S. Deng, W. Xiao, and N. Zhang, Solid State Sci. **13**, 1127 (2011).
16. H. S. Abbo and S. J. Titinchi, Appl. Catal. A: Gen. **435**, 148 (2012).
17. M. E. L. Preethi, S. Revathi, T. Sivakumar, D. Manikandan, D. Divakar, A. V. Rupa, and M. Palanichami, Catal. Lett. **120**, 56 (2008).
18. F. Shi, Y. Chen, L. Sun, L. Zhang, and J. Hu, Catal. Commun. **25**, 102 (2012).
19. T. A. Alsalim, J. S. Hadi, E. A. AlNasir, H. S. Abbo, and S. J. Titinchi, Catal. Lett. **136**, 228 (2010).
20. X. Qi, J. Li, T. Ji, Y. Wang, L. Feng, Y. Zhu, X. Fan, and C. Zhang, Microporous Mesoporous Mater. **122**, 36 (2009).
21. M. M. Treacy and J. B. Higgins, Collection of simulated XRD powder patterns for zeolites, Access Online via Elsevier (2001).
22. J. W. Richardson, J. V. Smith, and J. J. Pluth, J. Phys. Chem. **94**, 3365 (1990).
23. J.-S. Chen, W.-Q. Pang, and R.-R. Xu, Top. Catal. **9**, 93 (1999).
24. L. Xiao, J. Li, X. Shen, J. Yu, W. Pang, and R. Xu, Microporous Mesoporous Mater. **84**, 21 (2005).
25. H. Liu, G. Lu, Y. Guo, Y. Guo, and J. Wang, Nanotechnology **17**, 997 (2006).
26. I. Braun, G. Schulz-Ekloff, D. Wöhrle, and W. Lautenschläger, Microporous Mesoporous Mater. **23**, 79 (1998).
27. E. R. Cooper, C. D. Andrews, P. S. Wheatley, P. B. Webb, P. Wormald, and R. E. Morris, Nature **430**, 1012 (2004).
28. A. T. Stone, Environ Sci. Technol. **21**, 979 (1987).
29. J.-S. Choi, S.-S. Yoon, S.-H. Jang, and W.-S. Ahn, Catal. Today **111**, 280 (2006).